that showed a reversal potential corresponding to the Nernst potential of the applied gradient of formate, and the resulting reversal potential with identical amounts of formate on both sides of the bilayer was zero (Fig. 3, A and C). Formate gradients were chosen so that the cis side of the lipid bilayer had a higher (200 mM) concentration than the trans side (19.6 mM), in order to emulate the cytoplasmic release of formate in high amounts by PFL. In subsequent experiments, the pH on the trans side (the "periplasmic side") was acidified by a stepwise addition of HCl. A strong effect occurred at pH 5.1, when the formate current abruptly ceased. This effect was reversible (fig. S3) and constitutes a direct observation of pH-dependent gating in FocA. Although the transition point is still far above the pH of 4.0 in the crystallization condition for *St*FocA, it falls clearly below the pH of 6.8 determined as the switch point for the growth medium (*12*). The difference might be explained by the influence of the charged membrane surface on the ion concentration and thus the pH value in its immediate surroundings, as commonly described with Gouy-Chapman theory (*21*, *22*).

This study confirms that FocA acts as a specific channel for anionic formate at higher pH and is gated in a pH-dependent manner. Gating is mediated through the N termini of the peptide chains that order and reorient in a concerted fashion, and one might speculate that protonation of a histidine might be the basis for pH sensing. Earlier functional studies in vivo proposed that FocA operates as a H^+/formate symporter at low pH (*8*). Although our electrophysiological studies cannot address this electroneutral process directly, we note that the observed gating leaves the transmembrane formate channel within FocA unobstructed. Formate in the periplasm can still cross the membrane to reach a vestibule that is sealed off from the cytoplasm only by the N-terminal helix (fig. S2). A possible mechanism for active uptake could thus involve a cycling of the individual protomers through the three conformational states, whereby a transient opening of the cytoplasmic vestibule would release a formate anion trapped there while export would be hindered by the transport-rate-limiting selectivity filter (fig. S2). Active transport would result if the conformational changes were triggered by proton translocation.

References and Notes

1. J. Knappe, G. Sawers, *FEMS Microbiol. Rev.* **75**, 383 (1990).
2. J. Cole, *FEMS Microbiol. Lett.* **136**, 1 (1996).
3. J. W. Wimpenny, J. A. Cole, *Biochim. Biophys. Acta* **148**, 233 (1967).
4. J. Macy, H. Kulla, G. Gottschalk, *J. Bacteriol.* **125**, 423 (1976).
5. S. Leonhartsberger, I. Korsa, A. Böck, *J. Mol. Microbiol. Biotechnol.* **4**, 269 (2002).
6. B. L. Berg, J. Li, J. Heider, V. Stewart, *J. Biol. Chem.* **266**, 22380 (1991).
7. R. G. Sawers, *Antonie Leeuwenhoek* **66**, 57 (1994).
8. B. Suppmann, G. Sawers, *Mol. Microbiol.* **11**, 965 (1994).
9. S. Clegg, F. Yu, L. Griffiths, J. A. Cole, *Mol. Microbiol.* **44**, 143 (2002).
10. W. B. White, J. G. Ferry, *J. Bacteriol.* **174**, 4997 (1992).
11. M. H. Saier Jr. *et al.*, *Biochim. Biophys. Acta* **1422**, 1 (1999).
12. R. G. Sawers, *Biochem. Soc. Trans.* **33**, 42 (2005).
13. M. Hakobyan, H. Sargsyan, K. A. Bagramyan, *Biophys. Chem.* **118**, 135 (2005).
14. R. Rossmann, G. Sawers, A. Böck, *Mol. Microbiol.* **5**, 2807 (1991).
15. Y. Wang *et al.*, *Nature* **462**, 467 (2009).
16. A. B. Waight, J. Love, D. N. Wang, *Nat. Struct. Mol. Biol.* **17**, 31 (2010).
17. P. Agre *et al.*, *J. Physiol.* **542**, 3 (2002).
18. R. M. Stroud, P. Nollert, L. Miercke, *Adv. Protein Chem.* **63**, 291 (2003).
19. Materials and Methods are available as supporting material on *Science* Online.
20. G. von Heijne, Y. Gavel, *Eur. J. Biochem.* **174**, 671 (1988).
21. S. Stankowski, *Biophys. J.* **60**, 341 (1991).
22. R. Aveyard, D. A. Haydon, *An Introduction to the Principles of Surface Chemistry* (Cambridge Univ. Press, Cambridge, 1973).

Acknowledgments. We thank the staff at beamline X06SA at the Swiss Light Source, in particular T. Tomizaki, for assistance with data collection and W. Hardt (ETH Zürich) for genomic DNA of *S. typhimurium*. R. Dutzler (University of Zürich) is acknowledged for helpful discussions. This work was supported by Deutsche Forschungsgemeinschaft (Ei-520/3 to O.E., An-676/1 to S.L.A.A., and IRTG 1478). The structural model and structure factors have been deposited with the Protein Data Bank (accession code 3Q7K).

Supporting Online Material

www.sciencemag.org/cgi/content/full/332/6027/352/DC1
Materials and Methods
Figs. S1 to S3
Table S1
References

14 October 2010; accepted 17 March 2011
10.1126/science.1199098

Specificity of *Drosophila* Cytonemes for Distinct Signaling Pathways

Sougata Roy, Frank Hsiung,* Thomas B. Kornberg†

Cytonemes are types of filopodia in the *Drosophila* wing imaginal disc that are proposed to serve as conduits in which morphogen signaling proteins move between producing and target cells. We investigated the specificity of cytonemes that are made by target cells. Cells in wing discs made cytonemes that responded specifically to Decapentaplegic (Dpp) and cells in eye discs made cytonemes that responded specifically to Spitz (the *Drosophila* epidermal growth factor protein). Tracheal cells had at least two types: one made in response to Branchless (a *Drosophila* fibroblast growth factor protein, Bnl), to which they segregate the Bnl receptor, and another to which they segregate the Dpp receptor. We conclude that cells can make several types of cytonemes, each of which responds specifically to a signaling pathway by means of the selective presence of a particular signaling protein receptor that has been localized to that cytoneme.

Cells in developing tissues are influenced by multiple signals that they process and integrate to control cell fate, proliferation, and patterning. An example is in the *Drosophila* wing imaginal disc, where cells depend on several signaling systems that are intrinsic to the disc. Decapentaplegic (Dpp), Wingless (Wg), Hedgehog (Hh), and epidermal growth factor (EGF) are produced and released by different sets of disc cells, and receipt of these signaling proteins programs their neighbors to develop and grow. The mechanisms by which morphogen signaling proteins influence target cells must ensure both specificity and accuracy, and one possibility is that these proteins transfer at points of direct contact (*1*). Imaginal discs are flattened sacs that have a monolayer of columnar cells on one side and squamous peripodial cells on the other (Fig. 1, A and B). Many cells in wing discs make filopodial extensions that lie along the surfaces of the monolayers, oriented toward morphogen-producing cells (*2*). These extensions have been termed cytonemes to denote their appearance as cytoplasmic threads and to distinguish them as specialized structures that polarize toward morphogen-producing regions.

In wing discs dissected from third instar larvae, cytonemes can be seen as filaments extending from randomly generated somatic clones (*3*) (fig. S1) engineered to express a fluorescent protein such as soluble, cytoplasmic green fluorescent protein (GFP) (*2*, *4*) or a membrane-bound form such as mCD8:GFP (the extracellular and transmembrane domains of the mouse lymphocyte protein CD8 fused to GFP) (*5*). To image disc cytonemes, we placed unfixed discs peripodial side down on a coverslip, covered them with a 1-mm-square glass, and mounted them over a depression slide with the disc hanging from the

Cardiovascular Research Institute and Department of Biochemistry and Biophysics, University of California, San Francisco, CA 94158, USA.

*Present address: BioRad Laboratories, Hercules, CA 94547, USA.

†To whom correspondence should be addressed. E-mail: tkornberg@ucsf.edu

coverslip [details in (*5*)]. Because fluorescence levels in cytonemes were low relative to background, recorded images were processed to increase intensity and were subjected to deconvolution (*3*). Expression of CD8:GFP in wing disc clones revealed cytonemes emanating from both the apical and basal surfaces of columnar cells, as well as from peripodial cells (whose apical and basal surfaces could not be distinguished) (Fig. 1, A and B; fig. S1, A to C; and table S1). Most cytonemes were perpendicular to the anterior/posterior (A/P) axis of the disc and oriented toward the cells that produce Dpp at the A/P compartment border; others were oriented toward the cells that produce Wingless at the dorsal/ventral (D/V) compartment border (*5*). Disc-associated myoblasts also had filopodia (fig. S1D).

In the eye disc, cells in the columnar layer organize into ommatidial clusters as a wave of differentiation [the morphogenetic furrow (MF)] passes from posterior to anterior (Fig. 1C) [reviewed in (*6*)]. A second axis, centered at the equator, is orthogonal to the MF and defines a line of mirror-image symmetry where dorsal and ventral ommatidia are juxtaposed [reviewed in (*7*)]. The columnar cells divide during the third instar period but stop or divide only once after the MF passes. We induced CD8:GFP expression in somatic clones and examined the columnar cells. Whereas clones of six to eight cells were present on both sides of the MF, only cells anterior to the MF had visible cytonemes. Cytonemes emanating from these clones oriented either toward the axis defined by the MF or toward the axis defined by the equator (Fig. 1, D and E). Single clones with cytonemes oriented both toward the MF and toward the equator were not observed, and there was no apparent correlation between clone position and cytoneme orientation or cytoneme length (Fig. 1C). Cells in the peripodial layer of the eye disc also had cytonemes (fig. S1E).

The EGF pathway is a key signaling system for eye development [(*8*); reviewed in (*9*)], and cells in the MF express the EGF protein Spitz [Spi (*10*)]. Because one of the two types of anterior cell cytonemes extended toward the MF (Fig. 1D) and to explore the distribution of membrane-bound receptor proteins, we induced clones that expressed an epidermal growth factor receptor:GFP [EGFR:GFP (*11*)] fusion protein. Anterior cells expressing EGFR:GFP had cytonemes that oriented toward the MF, and most of these cytonemes had fluorescent puncta (Fig. 1F); no cytonemes that were marked by EGFR:GFP oriented toward the equator ($n = 125$ clones). Other than their "furrow-only" orientation, the cytonemes marked by EGFR:GFP were similar to those marked by CD8:GFP. In contrast, co-expression of CD8:GFP with (nonfluorescent) EGFR marked both furrow-directed and equator-directed cytonemes (fig. S1, G and H). Thus, expression of EGFR:GFP does not eliminate the equator-directed cytonemes, suggesting that the specific localization of EGFR:GFP to furrow-directed cytonemes is not a consequence of ectopic (over)expression of this fusion protein.

Evidence that the furrow-directed cytonemes depend on Spi/EGF signaling was obtained by expressing a dominant negative form of EGFR (*12*). Although EGFR is required for cell proliferation in the disc, small clones expressing $EGFR^{DN}$ (*12*) were recovered that co-expressed $EGFR^{DN}$ and CD8:GFP; in these clones, only cytonemes that appeared to be randomly oriented were present (Fig. 1G), indicating that the long, furrow-directed cytonemes (Fig. 1, D and F) may require EGFR signal transduction in the cytoneme-producing cells.

Wing disc–associated tracheal cells also make cytonemes (*13*, *14*). The transverse connective (TC) is a tracheal tube that nestles against the basal surface of the wing disc columnar epithelium and that sprouts a new branch [the air sac primordium (ASP)] during the third instar period in response to Branchless (Bnl) expressed by the wing disc (Fig. 1, A and B, and fig. S1, I to K) (*14*). Tracheal tubes are composed of a monolayer of polarized cells whose apical surfaces line a lumen. Expression of CD8:GFP throughout the trachea (*btl-Gal4 UAS-CD8:GFP*) made it possible for us to detect GFP fluorescence in several types of cytonemes emanating from the basal surfaces of the TC and ASP. Cytonemes at the tip of the ASP (Fig. 1A and fig. S1K) (length range, 12 to 50 μm; average length of 23 μm) contained the Breathless (Btl); the *Drosophila* fibrobast growth factor receptor (FGFR) and appeared to contact disc cells that express Bnl (*14*). Short cytonemes (length range, 2 to 15 μm; average length of 8.5 μm) extended from the TC cells in the vicinity of the ASP (fig. S1J and table S1).

We tested whether Dpp, Spi, Bnl, and Hh affected wing disc, eye disc, and tracheal cytonemes differentially. Ubiquitous expression of Spi, Bnl,

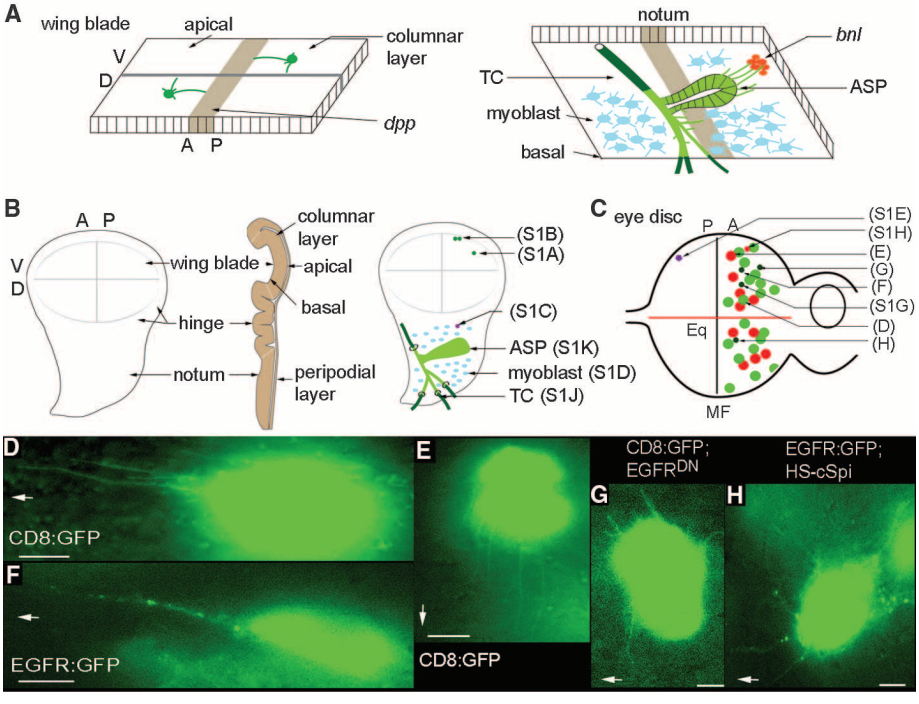

Fig. 1. Oriented cytonemes in the wing and eye discs. (**A**) Representation of cytonemes on the apical surface of the columnar layer of the wing disc (left) and of cytonemes at the basal surface of the wing disc emanating from the ASP (right). *bnl*- and *dpp*-expressing regions are in red and brown, respectively; the disc-associated Tr2 TC is partly external to the disc basal lamina (dark green) and partly within the disc basal lamina [light green (*12*)]; ASP is shown in light green; myoblasts, blue. (**B**) Drawings of third instar wing discs viewed from the columnar epithelial side (left), viewed through to the basal side (right), and viewed in cross section (middle). Positions of CD8:GFP-expressing clones cross-referenced (in parentheses) to supporting online material (SOM) figure panels. (**C**) Drawing of third instar eye–antennal disc with eye primordium to left, antenna primordium to right; equator, Eq; area posterior to MF, P; area anterior to MF, A. Approximate locations of CD8:GFP-expressing clones are shown [cross-referenced in parentheses to (D) to (H) and SOM figure panels] in the columnar layer with cytonemes directed toward the morphogenetic furrow (green), toward the equator (red), or in the peripodial layer (purple). Clones in overexpression genetic backgrounds are shown with small circles. (**D** and **E**) Cytonemes oriented toward the MF (D) or toward the equator (E) extended from anterior clones in the columnar layer. (**F**) An EGFR:GFP-expressing clone in the columnar layer illuminated puncta in cytonemes oriented to the MF. (**G**) A clone expressing CD8:GFP and $EGFR^{DN}$ extended short cytonemes. (**H**) EGFR:GFP-containing cytonemes radiate in many directions after ubiquitous expression of cSpi. In (D), and (F) to (H), MF is to left as indicated by arrows, and equator is down, as indicated by arrow in (E). Scale bars, 5 μm.

or Hh [induced by heat shock (Fig. 2, A and C to E) (*3*)] did not alter the A/P-oriented apical cytonemes in the wing disc, and, in the eye disc, the long cytonemes of the columnar layer were unaltered after ubiquitous expression of Dpp, Bnl, or Hh (Fig. 2, F, G, I, and J, and table S2). In contrast, long oriented cytonemes were absent in wing discs after ubiquitous expression of Dpp, and only short cytonemes that appeared to be randomly oriented were observed (Fig. 2B). Similarly, 0.5 to 3 hours after cSpi, a constitutively active form of EGF (*15*), was expressed ectopically by heat shock induction, clones expressing CD8:GFP in the eye disc had many short cytonemes that lacked apparent directional bias (Fig. 2H); in contrast to controls (Fig. 2F), no long cytonemes oriented toward the MF were observed. Cytonemes with normal orientation and length (including MF-directed cytonemes) were present in eye discs that were examined later, 8 hours after a pulse of cSpi expression (fig. S1F). To monitor EGFR-containing cytonemes for sensitivity and responsiveness to Spi, we expressed cSpi by heat shock induction and examined cells in clones expressing EGFR:GFP. After a pulse of cSpi expression, the extensions oriented outward without apparent directional bias, and the EGFR:GFP puncta were present in all cytonemes (Fig. 1, F and H).

To examine responses of the ASP tip cytonemes, we overexpressed Hh, Spi, Dpp, and Bnl by heat shock and examined GFP-marked cytonemes at the ASP tip (Fig. 2, K to P; tables S2 and S3; and fig. S2). No differences in number of cytonemes were detected until about 3 hours after heat shock. Four to 5 hours after heat shock, expression of Bnl increased the number of tip cytonemes by ~2.6 times, and although most of the cytonemes were <30 μm, the cytonemes >30 μm also increased (~3.2 times). Most of the long cytonemes in these preparations were oriented in directions other than toward the cells that normally express Bnl. The number of long cytonemes >30 μm did not change after overexpression of Hh, Spi, and Dpp (0.6 to 0.8 times); the number of short cytonemes increased after Dpp overexpression (~1.7 times) but not after overexpression of Hh or Spi.

Thus, the responses of apical wing disc cytonemes to overexpressed Dpp (Fig. 2, A and B), of eye disc cytonemes to ubiquitous Spi (Fig. 2, F and H), and of ASP tip cytonemes to exogenous Bnl (*Drosophila* FGF) (Fig. 2, K and N) (*14*) are similar. These results suggest that the cytonemes we detected in the wing discs and eye discs may have orientations and lengths that are dependent specifically on the respective sources of Dpp and Spi, whereas the ASP may extend cytonemes in response to more than one signaling protein. These results are, however, complicated by the heat shock mode of induction because both the cells that expressed GFP (and extended marked cytonemes) as well as the surrounding cells expressed the signaling proteins. To overcome this problem, we developed a method to induce two types of somatic clones in the same tissue, one that expressed GFP and another that expressed Dpp.

We used the GAL4 system to label cytonemes with CD8:GFP. Clones of GAL4-expressing cells were generated with heat shock–induced flippase (FLP recombinase). The second type of clone expressed a Dpp:Cherry fusion and was generated with a variant Cre-progesterone receptor recombinase that could be activated with a regime of heat shock and RU486 (*3*). By adjusting the timing and strength of induction, we produced wing discs with small, independent, and relatively infrequent clones. In discs with clones that expressed ectopic Dpp as well as clones that expressed CD8:GFP, apical cytonemes tagged with GFP were detected that oriented toward nearby Dpp:Cherry-expressing cells and not toward either the A/P or D/V signaling centers (Fig. 2, Q and R) (n = 5). Such "abnormally directed" cytonemes were never observed in control discs (n > 200). The abnormally oriented cytonemes suggest that apical cytonemes in the wing blade respond directly to sources of Dpp and that their orientation reflects extant sources of signaling protein.

To characterize the relationship between tracheal ASP tip cytonemes and FGF signaling from the wing disc, we examined the distribution of Btl (FGFR) in ASP cells and in ASP cytonemes. In preparations from larvae with tracheal expression of both CD8:GFP and Btl:Cherry (*btl-GAL4 UAS-CD8:GFP;UAS-Btl:Cherry*), cytonemes were marked by CD8:GFP, some of which had fluorescent Btl:Cherry puncta (Fig. 3A). Each ASP had only a few long (>30 μm) cytonemes, most of which contained Btl:Cherry puncta. Few of the more numerous short cytonemes (<30 μm) contained Btl:Cherry puncta. To characterize Btl:Cherry after overexpression of Bnl, we focused on preparations obtained 1 to 2 hours postinduction (genotype *btl-GAL4 UAS-CD8:GFP/HS-Bnl;UAS-Btl:Cherry/Gal80^{ts}*), because during this time interval the ASP morphology was close to normal but cytonemes had changed (Fig. 3, D to J, and table S4). We did not focus on ASPs after longer postinduction intervals because of major malformations to ASP morphology after 3 to 4 hours [fig. S3 and SOM; in contrast, changes to ASP cytonemes were not observed until 3 to 5 hours after overexpression of Bnl and CD8:GFP, and ASP morphology was normal at this time

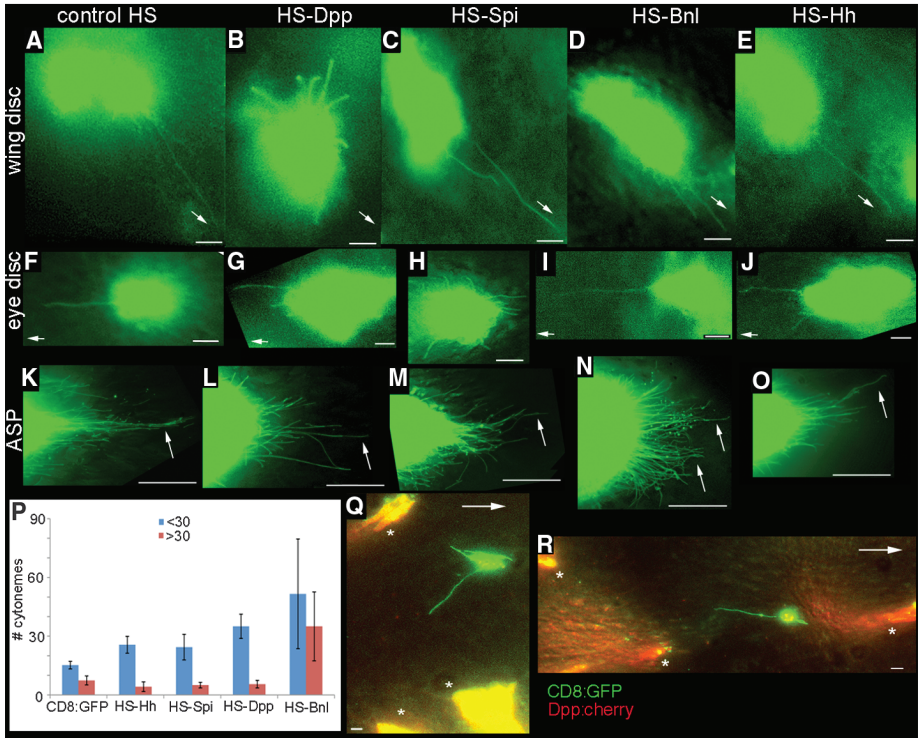

Fig. 2. Ligand-specificity of cytonemes. Dpp, Spi, Bnl, and Hh were expressed ubiquitously by heat shock 1/2 to 2 hours before imaging CD8:GFP in columnar cell clones in the wing disc (**B** to **E**), in columnar cell clones in the eye disc (**G** to **J**), or 3 to 5 hours before imaging CD8:GFP in ASPs in which expression was driven by *btl-Gal4* (**K** to **O**). CD8:GFP larvae heat-shocked although lacking the respective heat shock (HS) expression transgenes served as controls [(**A**), (**F**), and (K)]. (**P**) Chart tabulating number of long (>30 μm, red) and short (<30 μm, blue) cytonemes at the ASP tip (100-μm circumferential arc at the tip, average of five specimens, error bars represent SD). (**Q** and **R**) Images from wing discs with independent clones that express Dpp:Cherry (*) or CD8:GFP (green). Arrows point toward A/P signaling center [(A) to (E), (Q), and (R)], toward the MF [(F) to (J)], or to long cytonemes at the ASP tip [(K) to (O)]. Scale bars for (A) to (J), (Q), and (R), 5 μm; for (K) to (O), 30 μm.

interval for this genotype (Fig. 2)]. Long cytonemes with Btl:Cherry puncta were present 1 hour after a pulse of Bnl expression (Fig. 3E); but 2 hours after the pulse, most ASPs had no long cytonemes (Fig. 3F), and the number of short puncta-containing cytonemes increased at the tip (Fig. 3F) and along the shaft of the ASPs (Fig. 3G). After control heat shock or heat shock–induced expression of Dpp, the distribution of Btl:Cherry puncta in the ASP tip cytonemes was similar to normal controls: Long cytonemes had Btl:Cherry puncta, but most short cytonemes did not (Fig. 3, A to C, and table S4).

We also documented the distribution of Btl:Cherry in response to ectopic Bnl by imaging the entire ASP at lower magnification (Fig. 3, H to J). These views show Btl-containing puncta in the ASP cells and reveal an increase in number of puncta after induction of Bnl expression (per 20 ASP cells, the approximate number of Btl:Cherry puncta at the tip were 80 at time $t = 0$, 435 at $t =$ 1 hour, and 710 at $t = 2$ hours; in the middle region of the ASP numbers were 61 at $t = 0$, 415 at $t =$ 1 hour, and 750 at $t = 2$ hours). Two hours after Bnl expression was induced, the number of cytonemes increased all around the ASP periphery, and these cytonemes were densely populated with Btl:Cherry puncta (Fig. 3, H to J).

Because we found that the number of small cytonemes at the ASP tip may have increased after ectopic Dpp expression (fig. S2 and table S3), we investigated whether the *thickveins* (*tkv*) gene (*16*), which encodes a subunit of the Dpp receptor, is expressed in the ASP. We detected expression of the *tkv* reporter, *tkv-lacZ* (*P{lacW}tkv*^{16713}), in the ASP (fig. S4A). When we expressed Tkv:GFP and Btl:Cherry together, Tkv:GFP and Btl:Cherry segregated to separate tip cytonemes at the ASP tip (Fig. 3, K to M, and fig. S4, B to K). Whereas Tkv-containing cytonemes were short (<30 μm), most of the Btl-containing cytonemes were longer (three of four of the Btl:Cherry-containing cytonemes were longer than 30 μm), and they lay in focal planes closer to the disc (Fig. 3K, fig. S4H, and table S5). These properties were consistent in all preparations we examined in which both green Tkv and red Btl cytonemes were intact ($n = 29$). Imaging these marked ASPs revealed that overexpressed Tkv:GFP and Btl:Cherry were present not only in the plasma membranes (as expected) but also in separate puncta in the cell bodies (Fig. 3N and fig. S4, L to N). This shows that Tkv and Btl receptors also segregated to separate locations in the ASP cell bodies.

Our findings suggest that the ASP has long cytonemes that are specific to Bnl and specifically harbor Btl-containing puncta and that the ASP also has cytonemes that are specific to Dpp and specifically harbor Tkv. Similarly in the eye disc, the presence of EGFR:GFP in furrow-oriented cytonemes and not in equator-oriented cytonemes suggests that cytonemes in the eye disc also selectively localize receptors (Fig. 1F). And as we previously showed, apical cytonemes in the wing disc selectively localize Tkv (*5*). The apparent ligand specificities and contrasting make-up of these cytonemes suggest a diversity of functionally distinct subtypes: Cells appear to make cytonemes that respond specifically to the Dpp, EGF, or Bnl signaling proteins. [The basal filopodia implicated in Delta-Notch signaling in the wing disc (*17*) may represent yet another type.]

The mechanism that endows cytonemes with specificity for a particular signaling protein cannot be based solely on tissue-specific expression of a receptor. Spi, Dpp, and Hh are active in eye discs, but only changes in Spi signaling affected the furrow-directed cytonemes. And in the wing disc, both the Hh and EGF signal transduction pathways are active in cells at the A/P compartment border, but the apical cytonemes only responded to overexpressed Dpp. Our findings that tracheal cells in the ASP respond to both Dpp and Bnl and that the Tkv and Btl receptors are present in different cytonemes that the ASP cells extend suggest that specificity may be a consequence of the constitution of the cytoneme, not on which receptors the cells make. The mechanism that localizes receptors to different cytonemes is not known, but because the marked receptors we expressed also segregated to different intracellular puncta, the processes that concentrate these receptors in separate locations may not be exclusive to cytonemes. There is a precedent for segregation of proteins to different cellular extensions, neurons segregate proteins to dendrites or axons, so extending projections with specific and distinct attributes may be a general property of cells.

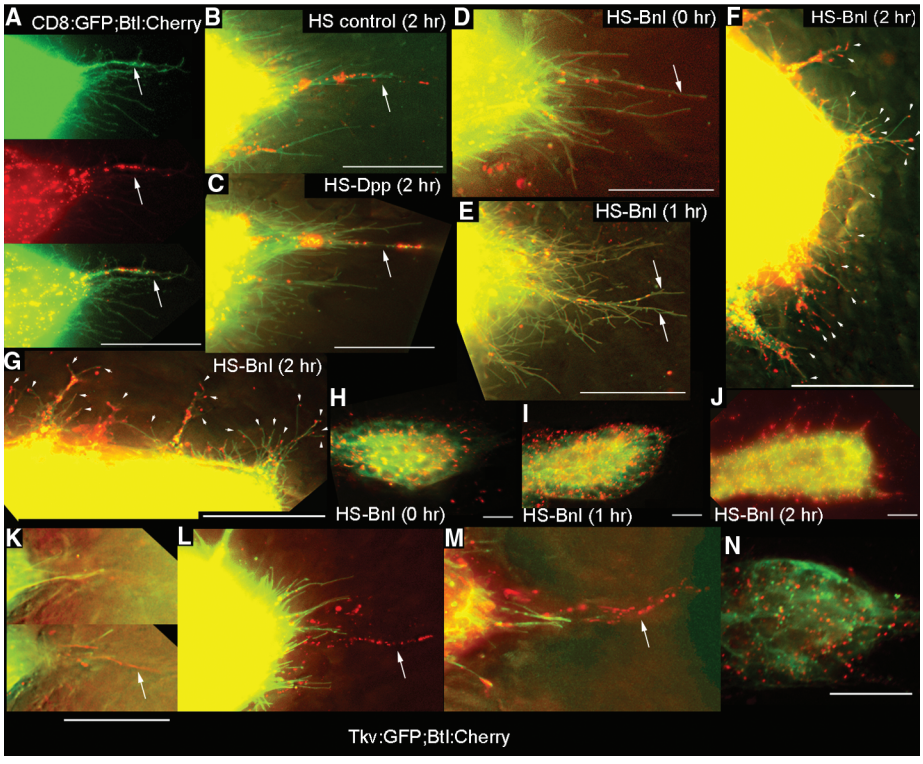

Fig. 3. Dpp and FGF receptors segregate to separate locations in the ASP. (**A** to **J**) Expression of Btl:Cherry and CD8:GFP driven by *btl-Gal4* mark ASP cytonemes (green) with Btl-containing puncta (red). [(A) and (B)] ASP tips from larvae lacking a HS transgene with (B) or without (A) heat shock. (C) Btl:Cherry puncta in ASP tip cytonemes after ectopic expression of Dpp. [(D) to (F) and (H) to (J)] Expression of Btl:Cherry and CD8:GFP released from Gal80^{ts} repression by temperature elevation (*3*) and subjected to heat shock for the indicated times. (E) Image of ASP tip 1 hour after heat shock. (F) Image of ASP tip 2 hours after heat shock [also see table S4 and (*3*)]. (G) Image of one side of the ASP tube between the TC and tip of (F). Arrowheads in (F) and (G) indicate short cytonemes containing Btl:Cherry puncta. [(H) to (J)] Low-resolution (40×) images showing distribution of Btl:Cherry after overexpression of Bnl. (F), (G), and (J) are images of the same preparation. (**K** to **N**) Tip of ASPs expressing Tkv:GFP and Btl:Cherry driven by *btl-Gal4*. (K) Two focal planes from z-sections in which Tkv:GFP-containing cytonemes were in a focal plane (top) less proximal to the disc than those with Btl:Cherry (bottom). [(L) and (M)] Projection images show distinct Tkv:GFP and Btl:Cherry–containing cytonemes at ASP tip. (N) Image of mid-distal ASP. Arrows in (A) to (D) and (K) to (M) indicate long cytonemes containing Btl:Cherry puncta. All images oriented ASP tip to right. Scale bars, 30 μm.

References and Notes

1. T. B. Kornberg, A. Guha, *Curr. Opin. Genet. Dev.* **17**, 264 (2007).
2. F. A. Ramírez-Weber, T. B. Kornberg, *Cell* **97**, 599 (1999).
3. Materials and methods are available as supporting material on *Science* Online.
4. T. T. Yang, L. Cheng, S. R. Kain, *Nucleic Acids Res.* **24**, 4592 (1996).
5. F. Hsiung, F. A. Ramirez-Weber, D. D. Iwaki, T. B. Kornberg, *Nature* **437**, 560 (2005).

6. J. Y. Roignant, J. E. Treisman, *Int. J. Dev. Biol.* **53**, 795 (2009).
7. R. Reifegerste, K. Moses, *Bioessays* **21**, 275 (1999).
8. J. P. Kumar, K. Moses, *Cell* **104**, 687 (2001).
9. C. Jones, K. Moses, *Semin. Cell Dev. Biol.* **15**, 75 (2004).
10. A. Schlesinger, A. Kiger, N. Perrimon, B. Z. Shilo, *Dev. Cell* **7**, 535 (2004).
11. D. Alvarado, A. H. Rice, J. B. Duffy, *Genetics* **167**, 187 (2004).
12. M. Freeman, *Cell* **87**, 651 (1996).
13. A. Guha, L. Lin, T. B. Kornberg, *Dev. Biol.* **335**, 317 (2009).
14. M. Sato, T. B. Kornberg, *Dev. Cell* **3**, 195 (2002).
15. R. Schweitzer, M. Shaharabany, R. Seger, B. Z. Shilo, *Genes Dev.* **9**, 1518 (1995).
16. E. Ruberte, T. Marty, D. Nellen, M. Affolter, K. Basler, *Cell* **80**, 889 (1995).
17. M. Cohen, M. Georgiou, N. L. Stevenson, M. Miodownik, B. Baum, *Dev. Cell* **19**, 78 (2010).

Acknowledgments: We thank H. Li and K. Kechris for help with data analysis; S. Liu for technical help; the Bloomington *Drosophila* Stock Center, I. Guerrero, E. Bier, M. Krasnow, J. Duffy, M. Sato, and K. Wharton for fly stocks; and T. Wunderlich for hCre*PR*. This work was supported in part by a Herbert Boyer Postdoctoral Fellowship (to S.R.) and by grants from the National Institute of General Medical Studies and the National Heart, Lung, and Blood Institute to T.B.K.

Supporting Online Material
www.sciencemag.org/cgi/content/full/332/6027/354/DC1
Materials and Methods
Figs. S1 to S4
Tables S1 to S5
References

12 October 2010; accepted 1 March 2011
10.1126/science.1198949

Noncanonical TGFβ Signaling Contributes to Aortic Aneurysm Progression in Marfan Syndrome Mice

Tammy M. Holm,[1]* Jennifer P. Habashi,[1,2]* Jefferson J. Doyle,[1]* Djahida Bedja,[3] YiChun Chen,[1] Christel van Erp,[1] Mark E. Lindsay,[1,2] David Kim,[1] Florian Schoenhoff,[1] Ronald D. Cohn,[1,2] Bart L. Loeys,[4] Craig J. Thomas,[5] Samarjit Patnaik,[5] Juan J. Marugan,[5] Daniel P. Judge,[6] Harry C. Dietz[1,2,6]†

Transforming growth factor–β (TGFβ) signaling drives aneurysm progression in multiple disorders, including Marfan syndrome (MFS), and therapies that inhibit this signaling cascade are in clinical trials. TGFβ can stimulate multiple intracellular signaling pathways, but it is unclear which of these pathways drives aortic disease and, when inhibited, which result in disease amelioration. Here we show that extracellular signal–regulated kinase (ERK) 1 and 2 and Smad2 are activated in a mouse model of MFS, and both are inhibited by therapies directed against TGFβ. Whereas selective inhibition of ERK1/2 activation ameliorated aortic growth, Smad4 deficiency exacerbated aortic disease and caused premature death in MFS mice. Smad4-deficient MFS mice uniquely showed activation of Jun N-terminal kinase–1 (JNK1), and a JNK antagonist ameliorated aortic growth in MFS mice that lacked or retained full Smad4 expression. Thus, noncanonical (Smad-independent) TGFβ signaling is a prominent driver of aortic disease in MFS mice, and inhibition of the ERK1/2 or JNK1 pathways is a potential therapeutic strategy for the disease.

The transforming growth factor–β (TGFβ) ligands belong to a family of cytokines that regulates diverse cellular functions, including proliferation, differentiation, and synthetic repertoire. TGFβ is secreted from cells as part of a large latent complex that binds to extracellular matrix (ECM) proteins including fibrillin-1 (*1*), the deficient gene product in Marfan syndrome (MFS). Current models posit that ECM sequestration of TGFβ inhibits its activation, thereby limiting its ability to stimulate cell surface receptors, TβRI and TβRII (*2*, *3*). In canonical signaling, the TβRI/II complex phosphorylates receptor-activated Smad2 and/or Smad3 (to pSmad2 and pSmad3, respectively), which leads to recruitment of Smad4, translocation to the nucleus, and the transcription of Smad-dependent genes (*4*). Recent work has shown that TGFβ also induces other (noncanonical) pathways, including the RhoA and mitogen-activated protein kinase (MAPK) cascades, the latter of which includes extracellular signal–regulated kinase (ERK), Jun N-terminal kinase (JNK), and p38 (*5*–*7*). TGFβ activates these by phosphorylation to pERK, pJNK, and pp38, respectively. In light of these findings, the exclusive focus on Smad signaling in TGFβ-related pathogenetic models needs to be reconsidered.

Increased Smad2/3 activation and increased expression of Smad-responsive genes (e.g., connective tissue growth factor and plasminogen-activator inhibitor–1, PAI-1) have been observed in the lung, skeletal muscle, mitral valve, and aortic wall in humans and a mouse model of MFS (*8*–*11*). Treatment of MFS mice with TGFβ-neutralizing antibody (TGFβNAb) ameliorates the phenotype in all of these tissues, in association with attenuated pSmad2/3 signaling (*8*–*11*). A similar rescue is achieved by using the angiotensin II type 1 receptor–blocker losartan (*8*–*11*), which is known to reduce the expression of TGFβ ligands, receptors, and activators (*12*–*14*). It has also been shown that mutations in TβRI or II, which lead to a paradoxical increase in pSmad2 signaling in the aortic wall, cause Loeys-Dietz syndrome, a condition that has considerable phenotypic overlap with MFS, including aortic aneurysm (*15*, *16*). Together, these earlier observations suggested that canonical TGFβ signaling drives disease pathogenesis in MFS. We have now explored the relative contributions of canonical and noncanonical TGFβ signaling cascades in MFS mice, by either genetically or pharmacologically inhibiting each cascade and analyzing the resultant phenotypic consequences.

We performed Western blot analysis on the proximal ascending aorta of 12-month-old mice heterozygous for a missense mutation in *Fbn1* (*Fbn1*$^{C1039G/+}$), a validated animal model of MFS (*17*). Compared with wild-type (WT) littermates, *Fbn1*$^{C1039G/+}$ mice showed a significant increase in activation of Smad2, ERK1/2, and MAPK kinase 1 (MEK1), the upstream activator of ERK1/2 ($P < 0.05$, $P < 0.001$, and $P < 0.05$, respectively) (Fig. 1A). In contrast, there was no difference in the activation of Smad3; JNK1; p38; ERK5; Rho-associated coiled-coil containing protein kinase–1 (ROCK1); or LIMK1, a downstream target of ROCK1 (Fig. 1A and fig. S1) (*18*). Furthermore, an in vivo trial of fasudil, a well-established inhibitor of the RhoA/ROCK pathway [details discussed in (*18*)] failed to attenuate aortic root growth in *Fbn1*$^{C1039G/+}$ mice (fig. S2).

Because TGFβNAb and losartan attenuate aortic root growth in *Fbn1*$^{C1039G/+}$ mice (fig. S3) (*10*), if Smad2 or ERK1/2 are important mediators of aortic disease in MFS, one would expect their activation to be reduced by these agents. Prior work demonstrated that Smad2 activation is decreased by both therapies (*10*). We now find that compared with placebo-treated littermates, *Fbn1*$^{C1039G/+}$ mice treated with either TGFβNAb or losartan also show a significant reduction in ERK1/2 activation ($P < 0.01$ for both) (Fig. 1B).

To confirm that ERK1/2 is a driver, rather than simply a marker, of aortic aneurysm progression, 2-month-old *Fbn1*$^{C1039G/+}$ mice were treated for 2 months with the selective MEK1/2 inhibitor RDEA119 (*19*). Aortic root size was measured by echocardiography at 2 months (baseline before treatment) and 4 months of age (Fig.

[1]Howard Hughes Medical Institute and Institute of Genetic Medicine, Johns Hopkins University School of Medicine, Baltimore, MD 21205, USA. [2]Division of Pediatric Cardiology, Department of Pediatrics, Johns Hopkins University School of Medicine, Baltimore, MD 21205, USA. [3]Department of Molecular and Comparative Pathobiology, Johns Hopkins University School of Medicine, Baltimore, MD 21205, USA. [4]Centre for Medical Genetics, Ghent University, 9000 Ghent, Belgium. [5]National Institutes of Health Chemical Genomics Center, Rockville, MD 20850, USA. [6]Department of Medicine, Johns Hopkins University School of Medicine, Baltimore, MD 21205, USA.

*These authors contributed equally to this work.
†To whom correspondence should be addressed. E-mail: hdietz@jhmi.edu.